Mineralogy and Petrology (2022) 116:349–368
https://doi.org/10.1007/s00710-022-00785-z

ORIGINAL PAPER

Geochemical and zircon U-Pb geochronological constraints on late mesozoic Paleo-Pacific subduction-related volcanism in southern Vietnam

Anh T.Q. Nong[1,3] · Christoph A. Hauzenberger[1] · Daniela Gallhofer[1] · Etienne Skrzypek[1] · Sang Q. Dinh[2]

Received: 5 August 2021 / Accepted: 7 June 2022 / Published online: 22 July 2022

Abstract
Late Mesozoic volcanic rocks comprising mainly basalt and basaltic-andesite to dacite occur in south-central Vietnam (Dalat zone) and to a lesser extent in southwestern Vietnam (Bay Nui area). Mineral and whole-rock chemistry indicate a calc-alkaline affinity for samples in the Dalat zone and a high-K calc-alkaline to shoshonitic affinity for rocks in the Bay Nui area. Mineral characteristics and variation diagrams of selected elements suggest that fractional crystallization dominated during magma differentiation. The Bay Nui volcanic rocks generally are more enriched in potassium and LILEs (large-ion lithophile elements) than volcanic rocks from the Dalat zone, which may indicate a more evolved nature or crustal assimilation. The similar chemical characteristics and eruption/emplacement age range of volcanic and plutonic rocks (ca. 90–110 Ma) of equal silica concentration indicate that the magma feeding the volcanic eruptions had the same source as that of the plutonic rocks. The observed mineral and whole-rock compositions with enrichment in LILEs, depletion in HFSEs (high field strength elements), and noticeably negative Nb, Ta, and Ti anomalies are characteristic for arc signatures. Zircon U-Pb geochronological data for the volcanic rocks indicate an age range of 95–105 Ma for the eruption. These geochemical and geochronological data link this Late Mesozoic volcanism with continental arc magmatism driven by the subduction of the Paleo-Pacific beneath eastern Indochina. Zircon xenocrysts with a likely magmatic origin cluster around 350 Ma and 250 Ma, indicating two earlier magmatic events most likely related to the subduction of the Paleo-Tethys beneath western Indochina and the subsequent Indosinian orogeny.

Keywords Southern Vietnam · Volcanic rocks · Geochemistry · Geochronology · Paleo-Pacific

Introduction

Andesitic volcanism is commonly associated with convergent margins and has been considered to significantly contribute to continental crust formation (Anderson 1976; Eichelberger 1978; Tatsumi et al. 2015; Chen and Zhao 2017). Therefore, a geochemical and geochronological study of volcanic rocks with a broadly andesitic composition is likely to provide crucial clues to the regional subduction settings that generated the volcanic activity. Along the eastern margin of Asia, voluminous Mesozoic volcanic rocks with a wide range of chemical compositions, isotopic signatures, and age data have been interpreted to originate from a subduction regime (Zhou and Li 2000; Liu et al. 2020). Along eastern Indochina, the Dalat zone (Vietnam) is considered to be part of the continental magmatic arc that resulted from the subduction of the Paleo-Pacific Ocean beneath eastern Asia during the Mesozoic and which extends from the northeastern margin of China to southwestern Borneo (Zhou and Li 2000; Nguyen et al. 2004; Thuy et al. 2004; Zhou et al. 2006; Morley 2012; Shellnutt et al. 2013) (Fig. 1). A large number of Late Mesozoic volcanic and plutonic bodies are distributed in southern Vietnam, particularly in the Dalat zone, while only a small volume is exposed in the Bay Nui

Editorial handling: Q. Wang

✉ Christoph A. Hauzenberger
christoph.hauzenberger@uni-graz.at

Anh T.Q. Nong
ntqanh@hcmus.edu.vn

[1] Institute of Earth Sciences – NAWI Graz Geocenter, University of Graz, Universitaetsplatz 2, 8010 Graz, Austria

[2] South-Vietnam Geological Mapping Division, 200 Ly Chinh Thang Street, District 3, Ho Chi Minh City, Vietnam

[3] Present Address: Faculty of Geology, University of Science, Vietnam National University Ho Chi Minh City, 227 Nguyen Van Cu Street, District 5, Ho Chi Minh City, Vietnam

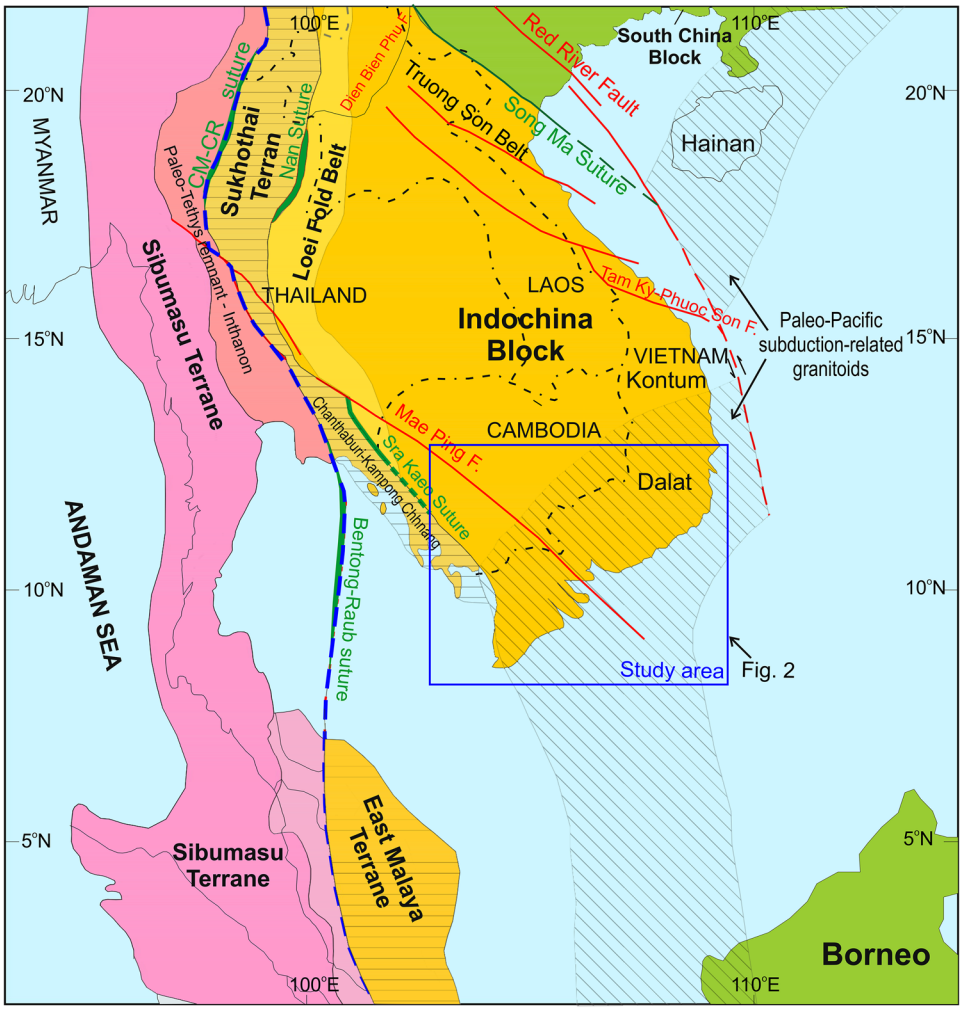

Fig. 1 Sketch map of mainland Indochina and adjacent areas showing Mesozoic magmatic belts associated with the closure of Paleo-Tethys and Paleo-Pacific subduction (modified after Sone and Metcalfe 2008; Fyhn et al. 2016)

area (SW Vietnam), which is separated from the Dalat zone by the Mae Ping Fault. Therefore, the Dalat zone has been the main focus of previous studies while the southwestern area around Bay Nui has received less attention (Bao 2000; Nguyen et al. 2004). A report on tectonics and metallogeny in southern Vietnam has presented whole-rock chemistry and Ar-Ar and Rb-Sr isotopic data of volcanic samples, yet only on a limited scale for the Deo Bao Loc area (Dalat zone) (Bao 2000). In the report, Mesozoic volcanics in southern Vietnam referred to as the Deo Bao Loc Formation, have been connected with Late Mesozoic subduction. However, a correlation between volcanic and plutonic rocks has not been drawn. Furthermore, the volcanic rocks distributed throughout the Dalat zone and those from the Bay Nui area have not yet been subject to a detailed chemical and geochronological study although the plutonic rocks in these two areas have distinct geochemical and geochronological characteristics (Nong et al. 2021).

Considering the lack of geochemical and geochronological data for volcanic rocks in southern Vietnam, particularly in the Bay Nui area (SW Vietnam), we present new mineral chemistry, whole-rock geochemistry, and zircon U-Pb data to differentiate between volcanic rocks in the Dalat zone (including the Tan Cang, Vung Tau, Hoa An, Phuoc Tan, Nui Gio, Deo Bao Loc localities) and in the Bay Nui area. The genetic relationship between volcanic and plutonic rocks in the study area within the Late Mesozoic tectonic framework in southern Vietnam is illustrated based on the comparison of their whole-rock compositions and ages. Furthermore, this study provides insights into eruption ages of volcanic rocks and also presents U-Pb dates of zircon xenocrysts, which were used for a regional correlation with tectono-magmatic events in Indochina and adjacent areas.

Geological setting

Regional outline and geology of the study area

The Indochina terrane is regarded as the largest continental plate in Sundaland (SE Asia) where two main tectonic events occurred during the Late Paleozoic-Mesozoic: (1)

the Indosinian orogeny (Late Paleozoic-Early Mesozoic) attributed to the Indochina-Sibumasu and Indochina-South China craton amalgamations as a result of the closure of Paleo-Tethys branches on the western and northeastern margin of Indochina, respectively and (2) the Yanshanian orogeny (Late Mesozoic) assigned to the subduction of the Paleo-Pacific beneath the eastern margin of Indochina (Hall 2012; Metcalfe 2017). Indochina is bordered by the South China block to the northeast along the "North Orogenic Belt" of the Song Ma suture zone, and by Sibumasu to the west along the Chiang Mai-Chiang Rai/Bentong-Raub suture zone (Fig. 1). The intermediate Inthanon zone contains Paleo-Tethyan remnants preserved after the amalgamation of Sibumasu and Indochina (Sone and Metcalfe 2008; Zaw et al. 2014; Metcalfe 2017).

The Loei Fold Belt and Sukhothai terranes along the western margin of Indochina are widely accepted to be magmatic arcs formed during the subduction of the Paleo-Tethys beneath Indochina (Zaw and Meffre 2007; Kamvong et al. 2014; Zaw et al. 2014; Nualkhao et al. 2018; Nong et al. 2022). The Loei Fold Belt mainly comprises Late Permian-Triassic andesitic-rhyolitic volcanic rocks and subordinate Devonian-Carboniferous and Silurian magmatic rocks which bear signatures of a subduction environment (Zaw and Meffre 2007; Hunyek et al. 2020). Along the eastern Indochina margin, a number of Jurassic and Early–Mid-Cretaceous volcanic and plutonic rocks distributed throughout Sumatra, SE Borneo, Vietnam, and eastern China have been frequently linked with Paleo-Pacific subduction (Nguyen et al. 2004; Clements et al. 2011; Shellnutt et al. 2013; Nong et al. 2021).

Local geological background

To the north of the Dalat zone, Precambrian amphibolite to granulite facies metamorphic suites from the Kontum Massif are considered to be the basement of Indochina. Xenocrystic zircon grains indicate the existence of an underlying Precambrian basement (~ 1.8 Ga) in the Dalat zone (Nguyen 2003). To the southwest of the Dalat zone, Devonian to Carboniferous terrigenous sediments around the Bay Nui area are thought to represent the oldest sequence and are conformably overlain by Permian limestones (Tri and Khuc 2009). These Paleozoic sedimentary sequences are in turn overlain by Triassic felsic-intermediate volcanic formations, sandstones, and Jurassic mudstones and sandstones (Hoa et al. 1996). Late Mesozoic volcanic assemblages are usually described as sequences of volcanics and associated tuffs. During the Mesozoic, southern Vietnam experienced extensive plutonism and volcanism associated with the Indosinian orogeny and the Yanshanian orogeny (Tri and Khuc 2009).

The study area is located along the eastern margin of Indochina where Paleo-Pacific subduction dominantly took place during the Late Mesozoic (118 to 87 Ma) (Nguyen et al. 2004; Shellnutt et al. 2013; Nong et al. 2021). As a result, a Mesozoic magmatic arc formed and extended continuously from the Dalat zone to southernmost Vietnam. Although the prominent NW-SE-oriented Mae Ping fault has been considered to be the boundary between the Dalat zone and the SW Vietnam area, it does not significantly disrupt the continuation of this magmatic arc (Nong et al. 2021) (Fig. 2).

The Late Mesozoic granitoid bodies within the Dalat zone and to a lesser extent in southwestern Vietnam have been attributed to two main stages: (1) continental arc-related magmatism (ca. 110–90 Ma) and (2) within-plate magmatism associated with an extensional regime (83–75 Ma) (Shellnutt et al. 2013; Nong et al. 2021). Therefore, the granite belt in southeastern Indochina marks the transition from the subduction-dominated Mesozoic era to the rift-dominated Cenozoic era (Fyhn et al. 2016).

In the Dalat zone, volcanic rocks are mainly assigned to the Deo Bao Loc Formation and the Nha Trang Formation which contain tuffs of intermediate to acidic composition, respectively. Although these volcanic rocks are named differently according to their localities and variable compositions (i.e., Long Binh Formation and Don Duong Formation), they are believed to originate from a similar Late Mesozoic tectonic setting based on field relationships, petrographical characteristics, whole-rock chemistry, and Ar-Ar and Rb-Sr isotopic data (Bao 2000). In the Bay Nui area (southwestern Vietnam) Early Triassic rhyolite and rhyolitic tuffs are interbedded with a marine sedimentary sequence. Another Late Mesozoic volcanic activity has been recognized as comprising intermediate-felsic compositions (andesite, andesitic tuffs, and rhyolite) (Hoa et al. 1996).

Field relationships and petrography

Samples were collected from several quarries within the study area (e.g., Bay Nui, Tan Cang, and Hoa An quarries) (Fig. 3a). Xenoliths of Mesozoic granitoids (collected at the same localities and dated at ca.106 Ma by Nong et al. 2021) are occasionally found in basaltic andesite and volcanic tuffs in the Bay Nui area (Fig. 3b). Greenish-grey andesite is occasionally interbedded with strongly iron-stained andesites or calcite-rich layers in the Vung Tau area (Fig. 3c, d). In terms of structural geology, andesite from the Deo Bao Loc area exhibits fracturing parallel to the regional deformation trend (Fig. 3e, f). Additionally, volcanic rocks in southwestern Vietnam may cause metasomatism in Jurassic sedimentary rocks (Hoa et al. 1996).

Basaltic andesites with aphanitic or porphyritic textures prevail in the Bay Nui, Tan Cang, Vung Tau, Hoa An, and Phuoc Tan areas. Plagioclase, pyroxene, and subordinate amphibole usually occur as phenocrysts (Fig. 4a, b, e, f,

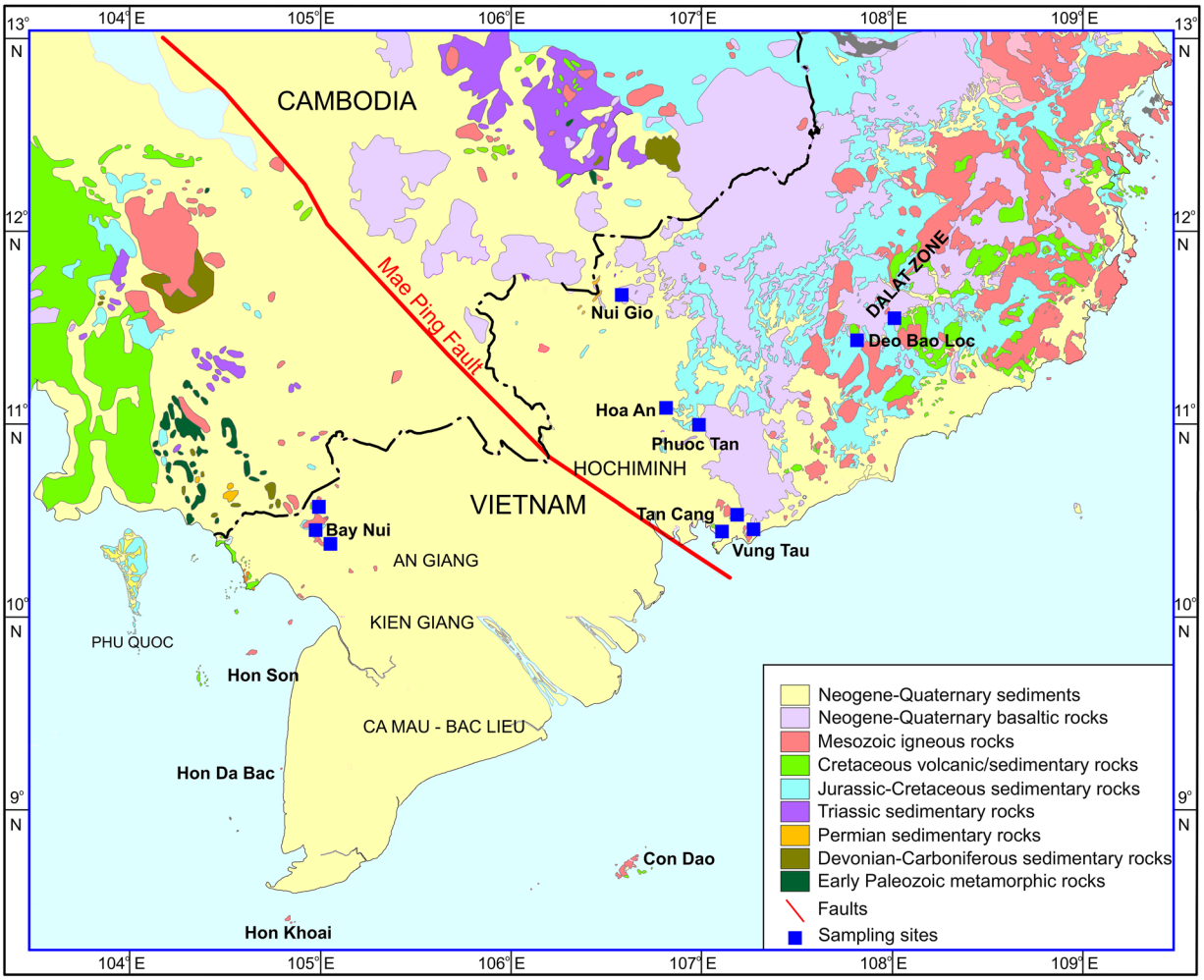

Fig. 2 Geological map of southern Vietnam and adjacent areas (modified after Tien 1991; Hoa et al. 1996)

and g). A porous structure is locally observed in the rocks with pores filled with microcrystalline SiO_2 (Fig. S1 in the ESM - electronic supplementary material). Accessory phases are apatite, titanite, and magnetite. Chlorite and epidote are the most common secondary minerals.

Andesitic tuffs occur throughout the Bay Nui, Phuoc Tan, and Nui Gio areas. They comprise volcanic ash and fragments of various rock types, e.g., sedimentary, plutonic rocks, and volcanic fragments of basaltic andesite (Fig. 4c, d). Andesitic tuffs from the Phuoc Tan and the Nui Gio areas exhibit strong chloritization and epidotization where relicts are hardly observed.

Porphyritic andesite and dacite are commonly found in the Deo Bao Loc area. They contain more amphibole compared to those of the other areas with prominent phenocrysts of plagioclase and amphibole embedded in fine-grained plagioclase and glassy groundmass (Fig. 4h). Accessory phases are apatite, ilmenite, titanite, and sulfide minerals (e.g., pyrite and arsenopyrite) (Fig. S1 in the ESM). Chlorite and epidote are common secondary phases.

Rhyolite occurs sporadically in the study area and was collected only from the Bay Nui and Vung Tau areas. It displays scattered fresh quartz and plagioclase phenocrysts in a felsic groundmass.

Analytical methods

Thirty volcanic samples representative of seven geological sites were collected in southern Vietnam. Ten were used for quantitative mineral analyses. Microtextures, backscattered-electron (BSE) images, and mineral compositions were investigated with a JEOL JXA-8530 F Plus electron probe microanalyzer (EPMA) using wavelength-dispersive X-ray spectrometry (WDS). Thin sections were coated with carbon and analyzed at an accelerating voltage of 15 kV, 10 nA beam current, ~ 1–3 µm beam diameter,

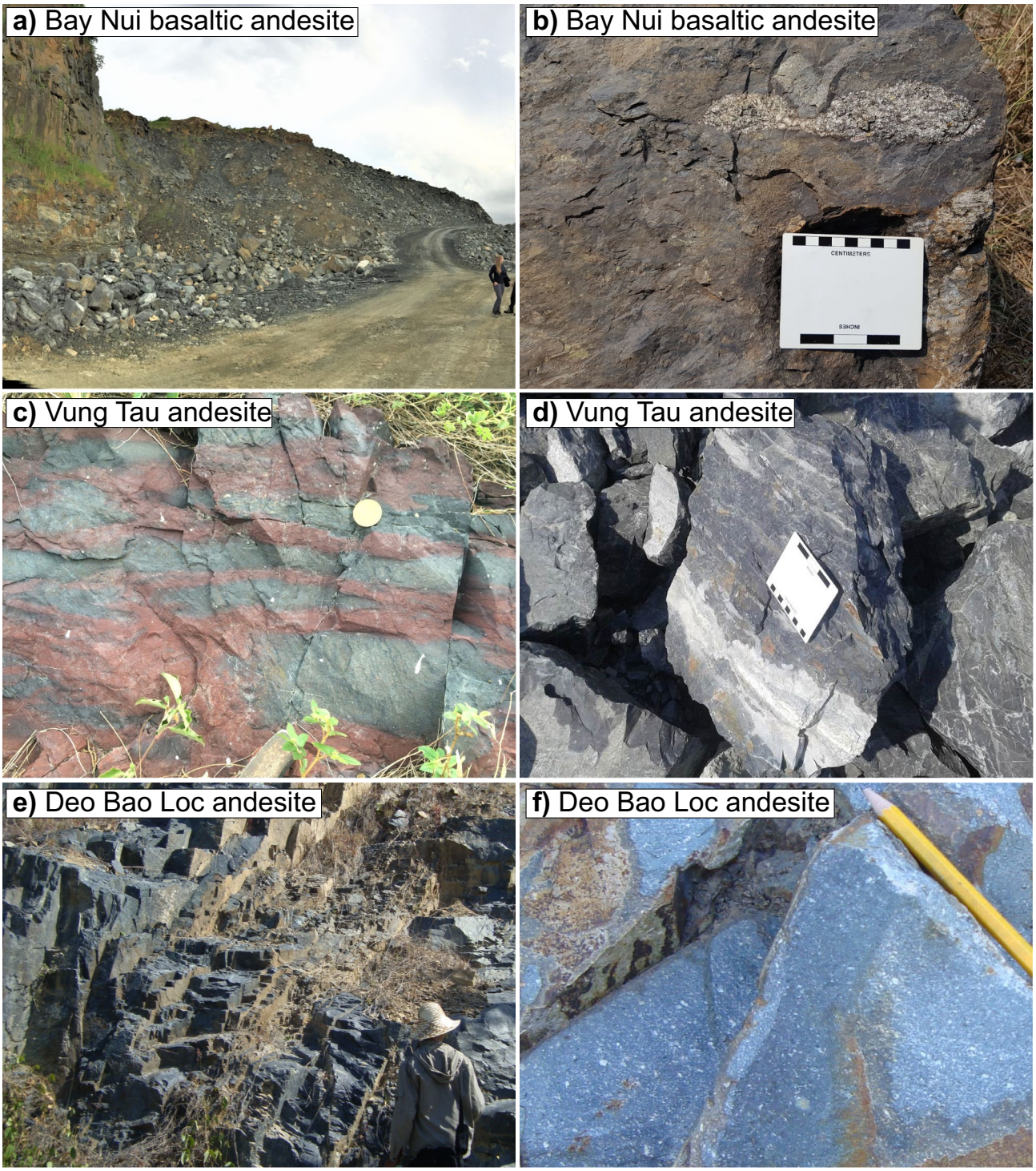

Fig. 3 Outcrop features of the studied rocks: **a** Basaltic andesite from a quarry in the Bay Nui area; **b** Basaltic andesite containing xenoliths of Late Mesozoic granitoids (Nong et al. 2021); **c** Greenish-grey andesite interbedded with strongly iron-stained andesite; **d** Calcite-rich andesite layers; **e** Fractures following the regional deformation trend; **f** Porphyritic andesite containing plagioclase phenocrysts

and counting times of 20 s on peak and 20 s for total background. The ZAF correction method was applied to all analyses and the following reference materials and X-ray lines were used for calibration: garnet (Fe Kα, Mg Kα, Ca Kα), titanite (Ti Kα), chromite (Cr Kα), rhodonite (Mn Kα), albite (Na Kα), microcline (K Kα, Si Kα, Al Kα), F-phlogopite (F Kα), and tugtupite (Cl Kα). The detection limits of major elements are 0.02%.

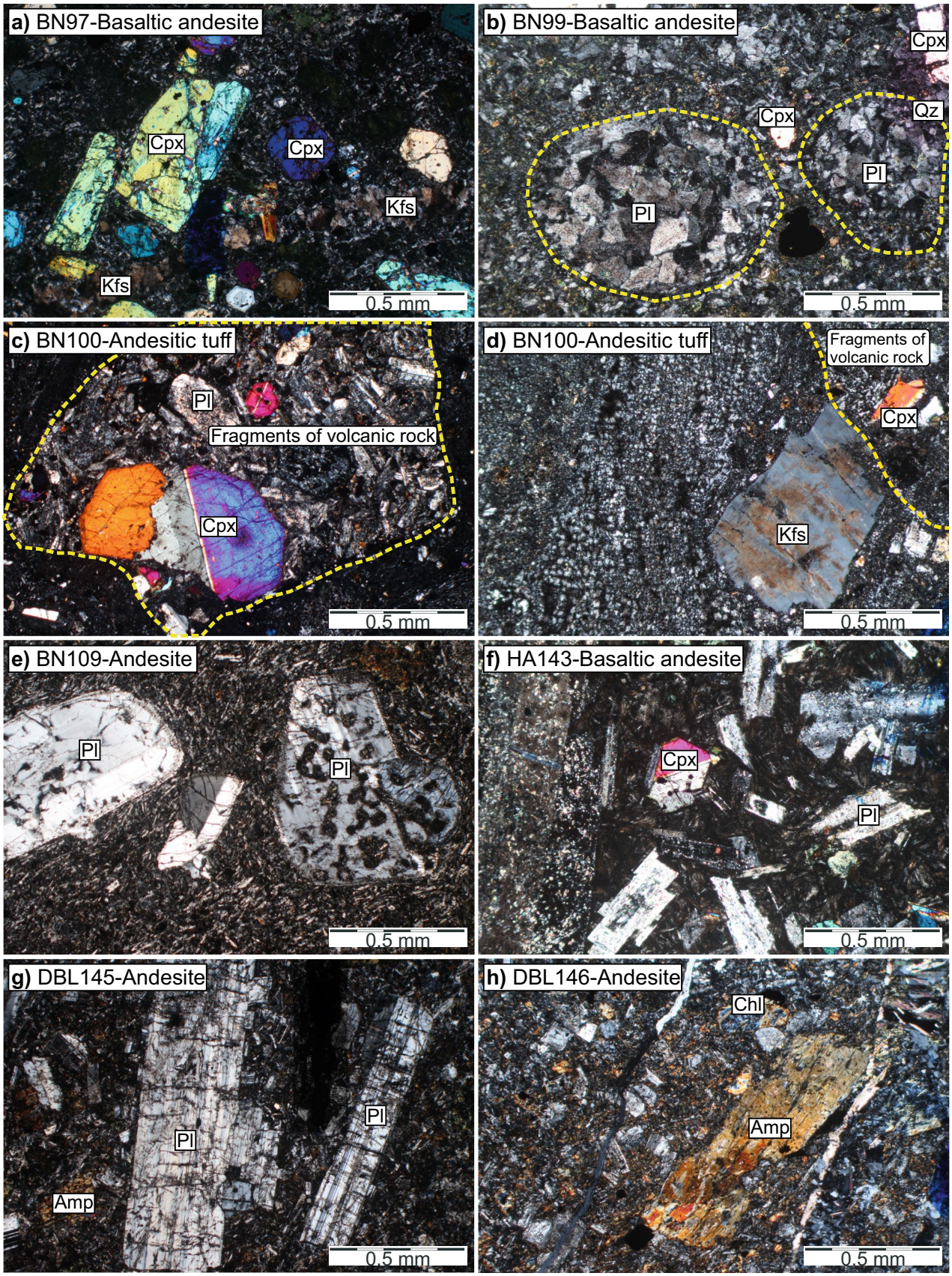
a) BN97-Basaltic andesite
Cpx
Cpx
Kfs
Kfs
0.5 mm
b) BN99-Basaltic andesite
Cpx
Cpx
Qz
Pl
Pl
0.5 mm
c) BN100-Andesitic tuff
Pl
Fragments of volcanic rock
Cpx
0.5 mm
d) BN100-Andesitic tuff
Fragments of volcanic rock
Cpx
Kfs
0.5 mm
e) BN109-Andesite
Pl
Pl
0.5 mm
f) HA143-Basaltic andesite
Cpx
Pl
0.5 mm
g) DBL145-Andesite
Pl
Pl
Amp
0.5 mm
h) DBL146-Andesite
Chl
Amp
0.5 mm

◂**Fig. 4** Cross-polarized light images of minerals: **a** Pyroxene phenocrysts in basaltic andesite (Bay Nui area); **b** Assemblage of anhedral to subhedral plagioclase (Bay Nui area); **c** Fragments of volcanic rock in andesitic tuff (Bay Nui area); **d** K-feldspar xenocryst in andesitic tuff (Bay Nui area); **e** Gnawed plagioclase phenocrysts in andesite (Bay Nui area); **f** Plagioclase forming intersertal texture in basaltic andesite (Hoa An area); **g** Euhedral plagioclase phenocrysts in andesite (Deo Bao Loc area); **h** Subhedral amphibole phenocryst in andesite (Deo Bao Loc area). Abbreviations of mineral names follow Whitney and Evans (2010): Cpx – Clinopyroxene, Kfs – K-feldspar, Pl – Plagioclase, Qz – Quartz, Amp – Amphibole, and Chl – Chlorite; and areas: BN – Bay Nui, HA – Hoa An, and DBL – Deo Bao Loc

Twenty-four samples were milled using a tungsten carbide vibratory disc mill. For tuff samples, wall rock fragments were removed before powdering for geochemical analyses. The powdered samples were dried at 105°C for at least 4 h in an oven. Loss on ignition (LOI) was carried out by igniting ~ 1 g of each sample in ceramic crucibles at 1030°C for 1 h.

Samples for major element determination were analyzed by X-ray fluorescence spectroscopy (XRF). Glass beads of ~ 4 cm diameter were prepared by melting 1 g of rock powder and 7 g of di-lithium tetraborate powder in platinum crucibles. The glass beads were analyzed with a Bruker Tiger S8-II XRF spectrometer with an Rh target X-ray tube to obtain major, minor and selected trace elements. The relative standard deviation of major elements (> 1 wt%) is 1–2% and that of minor and trace elements (0.02–1 wt%) is 3–5%.

For trace and rare earth elements, powdered samples (~ 40 mg) were dissolved with a mixture of 1 ml double distilled HNO_3 (15 N) and 2 ml suprapure HF (28 N) in Teflon beakers with tightly screwed caps on a hotplate at 180°C for 48 h. The solutions of samples were then evaporated and re-dissolved twice in 1 ml HNO_3 (15 N) and once in 1 ml HCl (12 N). An ultrasonic bath was used for full dissolution. The dissolved samples were then diluted in 2% HNO_3 to obtain the final ~ 1500x dilution for inductively coupled plasma-mass spectrometry (ICP-MS). Analyses were performed with an Agilent 7700 quadrupole ICP-MS system at the Institute of Chemistry, University of Graz. The standards BHVO-2 (USGS) and IV-ICPMS-71 A (Inorganic Ventures) were used for calibration and JR-2 and JG-3 (GSJ) were analyzed to monitor the accuracy of the measurements. The detection limit was 0.1 – 0.01 ppm for most trace elements. Geochemical data were processed and plotted using the R-based software package GCDkit (Janoušek et al. 2006).

Five representative samples were selected for U-Pb zircon dating by laser ablation multi collector (MC) ICP-MS. The samples were crushed to reach a grain size of ca. 50–250 µm. Gold panning was then performed to concentrate the heavy minerals which were subsequently processed with a Frantz magnetic barrier separator. Handpicking of random zircon grains was performed under a binocular microscope. Zircon samples were mounted in epoxy resin and polished to expose the grain centers. Cathodoluminescence (CL) images of zircon, obtained with a JEOL JXA-8530 F Plus EPMA, were used for selecting analysis spots on zircon grains. An ESI NWR 193 nm laser ablation system coupled to a Nu Plasma II multi collector (MC) ICP-MS system was used for all analyses. The laser was operated at 5 or 8 Hz repetition rate and 20% of 5 mJ laser energy output resulting in a sample fluence of ~ 2.5 J/cm². The laser was warmed up by shooting 25 s at the shutter, which was followed by 15 or 30 s of sample ablation on each 25 µm diameter spot (see Table S1 in the ESM for detailed measurement conditions).

GJ1 zircon (Jackson et al. 2004) was used as the primary reference material. Plešovice (Sláma et al. 2008), 91,500 (Wiedenbeck et al. 1995), and M257 zircon samples (Nasdala et al. 2008) were used as secondary reference material to assess the reproducibility and accuracy of analyses. Secondary reference materials were analyzed once for every 6 or 13 analyses and gave an accuracy better than 2% and long-term reproducibility of 1.3%. No common lead correction was applied to the results. $^{206}Pb/^{238}U$ weighted mean ages for each sample were calculated from single zircon dates showing less than 5% discordance. The uncertainty of the mean ages was obtained by propagating systematic uncertainties to the uncertainty of the weighted mean age (Horstwood et al. 2016). Data reduction was performed with the IOLITE v. 3.71 software package and the X_U-Pb_Geochron4 DRS (Paton et al. 2010, 2011). Concordia diagrams and weighted mean calculations were performed with Isoplot (Toolkit for Microsoft Excel) (Ludwig 2008).

Results

Mineral chemistry

The majority of pyroxene and amphibole of volcanic rocks shows compositions similar to those of previously analyzed plutonic rocks (Nong et al. 2021), especially for CaO, MgO, and FeOt from EPMA analyses of rock-forming minerals. Figure 5a, c show the overlap of pyroxene and amphibole compositions between volcanic and plutonic rocks. Detailed analytical results are given in Supplementary Table S2 in the ESM.

Pyroxene: Basaltic andesite samples from the Bay Nui and the Hoa An areas (Dalat zone) usually contain clinopyroxene. The clinopyroxene phenocrysts and finer grains in the groundmass of rocks from Bay Nui are diopside and those from the Hoa An area are augite-diopside according to the classification diagram in Fig. 6a (Morimoto 1988). The X_{Mg} [$Mg/(Mg+Fe^{2+})$] is high and variably ranging from 0.5 to 0.9 while Cr_2O_3 content is generally low (< 0.1 wt%). The titanium versus Ca + Na diagram shows that the host magma of pyroxene of the Bay Nui rocks is more alkaline compared to the Hoa An rocks (Leterrier et al. 1982) (Fig. 6b). Pyroxene occasionally exhibits oscillatory zonation where

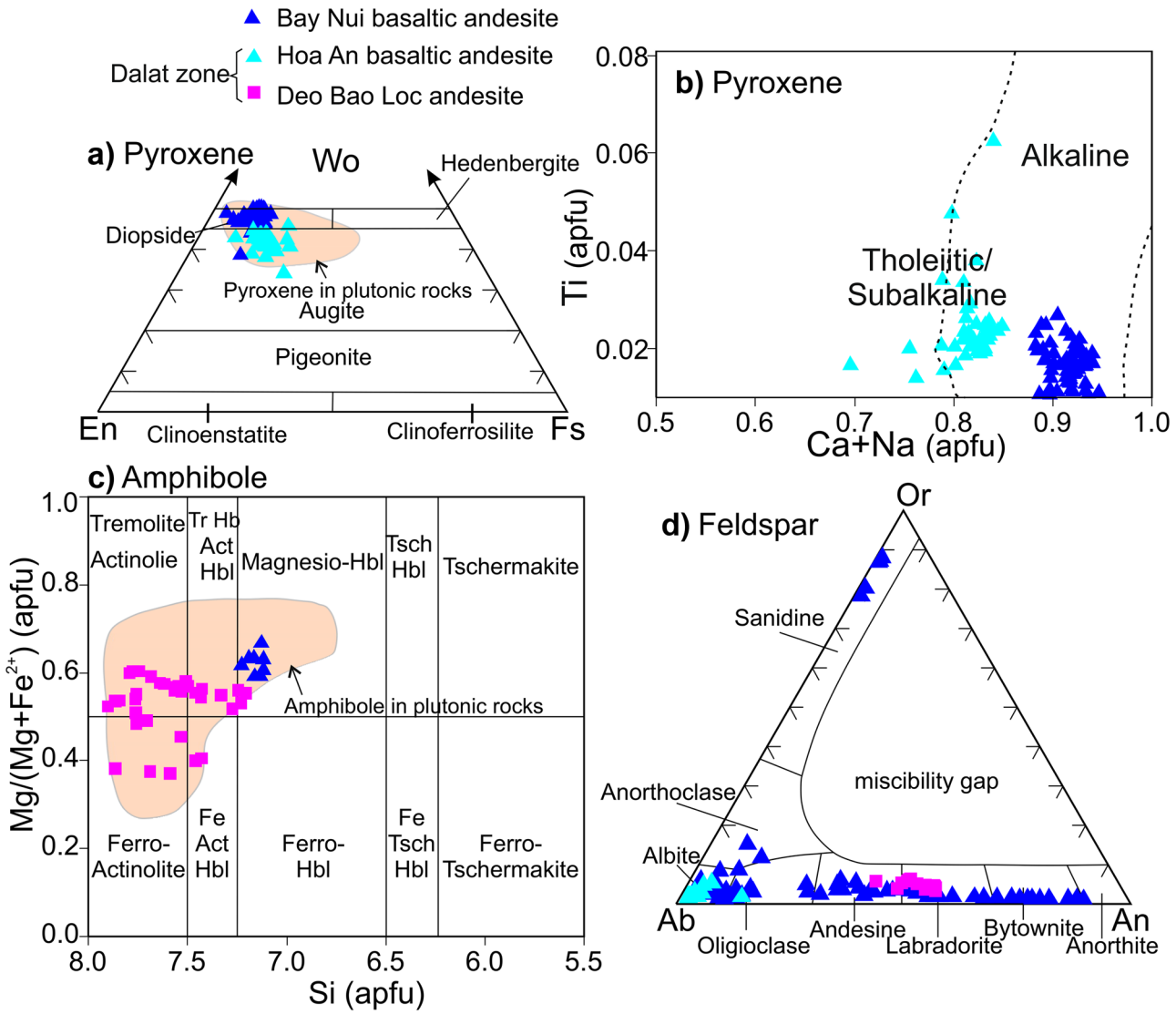

Fig. 5 Classification diagrams for volcanic rocks: **a** Total alkalis versus silica (Le Bas et al. 1986); **b** Nb/Y versus Zr/TiO_2 (Winchester and Floyd 1977); **c** K_2O versus SiO_2 diagram illustrating the compositional series (Peccerillo and Taylor 1976); and **d** Ternary diagram showing magmatic series (Irvine and Baragar 1971)

the outer zones are concentric rings and periodically repeat chemical compositions from the core.

Amphibole: is commonly found in the Deo Bao Loc andesite (Dalat zone) and occasionally in the Bay Nui rocks. Chemical compositions of amphibole belong to the calcic group with $(Ca+Na)^B > 1.00$ and $Na^B < 0.50$. Amphibole of the Deo Bao Loc andesite has a moderate MgO content and is classified as ferro- to magnesio-hornblende and actinolite according to amphibole nomenclature (Leake et al. 1997; Hawthorne et al. 2012) (Fig. 6c). Amphibole of the Bay Nui basaltic andesite has a higher MgO content than amphibole of the Deo Bao Loc andesite and is categorized as magnesio-hornblende. The halogen content (F and Cl) of all analyzed amphiboles is generally low (< 0.3 wt%).

Feldspar: Plagioclase of the Bay Nui basaltic andesite is characterized by a wide range of compositions (X_{An} = 0.1–0.8) while plagioclase composition is more restricted in the Hoa An basaltic andesite (X_{An}< 0.2) and the Deo Bao Loc andesite (X_{An} = 0.4–0.5) (Fig. 6d). Plagioclase usually shows normal zoning with calcium-rich cores and sodium-rich rims. K-feldspar has a low content of sodium (Na_2O < 2.32 wt%) and calcium (CaO < 0.24 wt%). Barium content is very low with a maximum of 0.1 wt%.

Biotite: Xenomorphic biotite is a common constituent of andesitic tuff. Chemical composition points to eastonite (high aluminum and magnesium) and a calc-alkaline orogenic tectonic setting of the host magma (Abdel-rahman 1994). The TiO_2 concentration is moderate (4.05–5.31

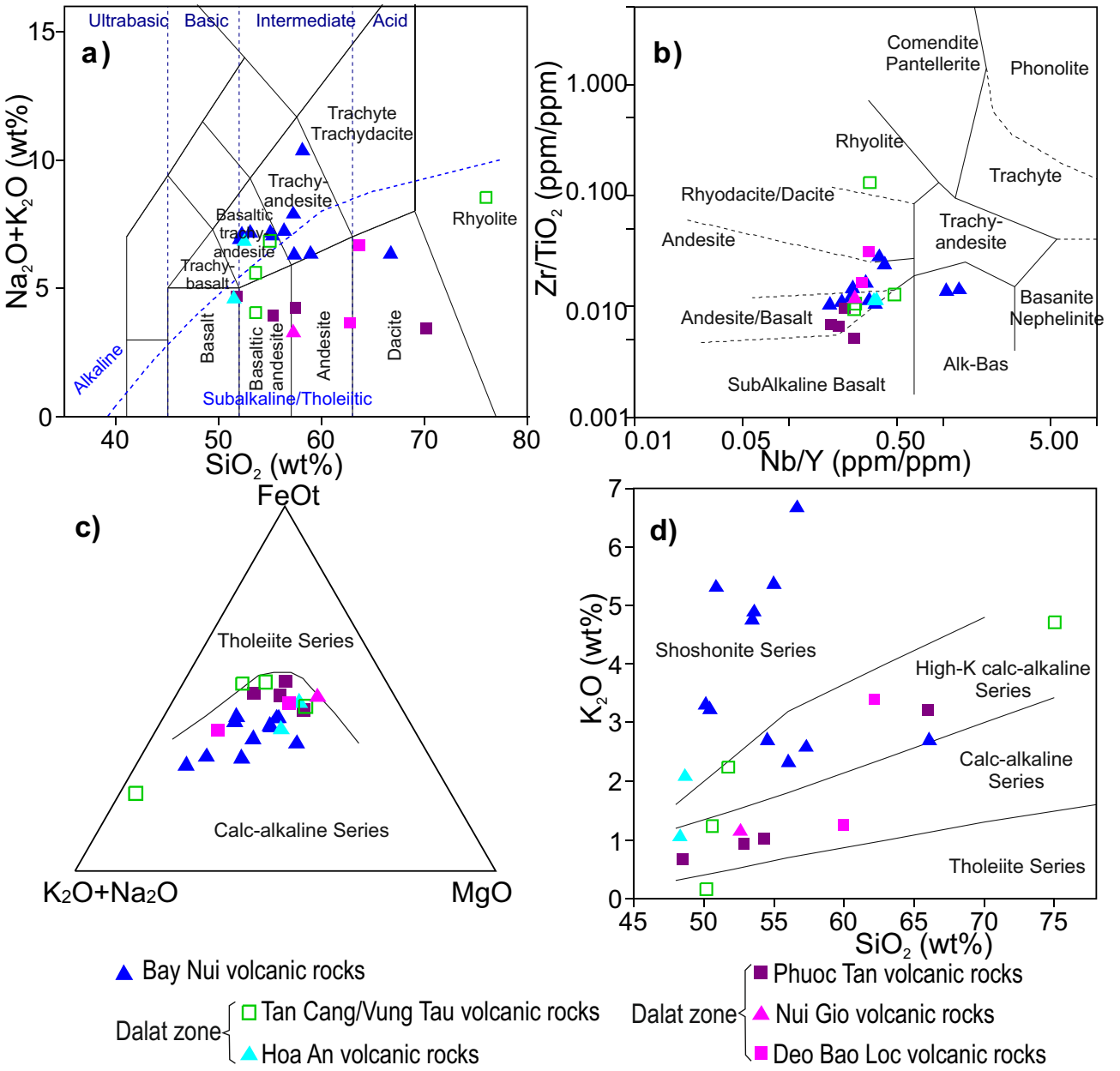

Fig. 6 Chemical composition of minerals from EPMA analyses: **a** Ca-Mg-Fe pyroxene classification diagram (Morimoto 1988): En – enstatite, Wo – wollastonite, Fs – ferrosilite; **b** Magma series are distinguished based on pyroxene chemical composition, the Bay Nui rocks are close to alkaline series while the Hoa An (Dalat) rocks represent subalkaline series (Leterrier et al. 1982); **c** Amphibole classification diagram for calcic amphiboles (Leake et al. 1997); and **d** An-Or-Ab feldspar classification, Ab – albite, Or – orthoclase, An – anorthite

wt%). Halogen composition shows enrichment of fluorine over chlorine with 1.14–1.64 wt% F and 0.04–0.08 wt% Cl.

Whole-rock chemistry

Major elements

In the rock classification diagrams (Fig. 5a, b), the samples span a large range from basaltic to rhyolitic composition but mainly fall into the basaltic/basaltic-andesitic to andesitic/trachyandesitic fields (Winchester and Floyd 1977; Le Bas et al. 1986). Alkali concentrations vary from subalkaline to alkaline and shoshonitic series (Irvine and Baragar 1971; Peccerillo and Taylor 1976) (Fig. 5c and d). Whole-rock compositions are presented in Supplementary Table S3 in the ESM.

In major element oxide versus SiO_2 variation diagrams, TiO_2, MgO, Fe_2O_3t, CaO, and P_2O_5 decrease with increasing SiO_2 content while K_2O does not show a clear correlation with SiO_2 (Fig. S2 in the ESM).

Trace elements

Harker diagrams (Fig. S2 in the ESM) of selected LIL elements (Rb, Ba, and Sr) define two groups: (1) high concentrations of LILEs are found in Bay Nui rocks and (2) lower contents of LILEs in the Dalat zone (Tan Cang, Vung Tau, Hoa An, Phuoc Tan, Nui Gio, Deo Bao Loc areas). Rubidium, Ba, and Sr negatively correlate with SiO_2 content in the Bay Nui samples while they positively correlate with SiO_2 in rocks of the remaining areas. All rock samples show a negative correlation of Cr with SiO_2 and a slightly positive correlation of HFSEs with SiO_2.

In the primitive mantle-normalized trace element diagrams (McDonough and Sun 1995), most of the samples, except for the Phuoc Tan samples (PT131–PT134) and one Vung Tau sample (VT140), are characterized by enrichment in Cs, Rb, and Ba. All samples show depletion in Nb, Ta, and Ti, which is commonly found in magmas with arc signatures (Fig. 7a, c) (e.g., McDonough 1991; Zheng 2019). Chondrite-normalized REE diagrams after Nakamura (1974) show enrichment of LREEs relative to HREEs (La/Yb = 3.92–20.12). Noticeably, Eu, the element preferentially incorporated into plagioclase, does not display a negative anomaly, with the exception of one rhyolite sample VT140, indicating that plagioclase fractionation was not significant (Fig. 7b, d).

Trace and rare earth elements of volcanic rocks are plotted together with plutonic samples of equivalent silica concentration from the corresponding areas in southern Vietnam, i.e., the Bay Nui volcanic samples are compared to the Bay Nui plutonic samples and the volcanic samples from the Dalat zone are compared to the Dalat plutonic samples (Nguyen 2003; Nong et al. 2021) (Fig. 7). The volcanic and plutonic rocks exhibit similarities in element patterns in the spider diagrams. In the Bay Nui area and the Dalat zone, apart from the Phuoc Tan samples and sample VT140, the volcanic samples display patterns well overlapping with those of plutonic samples. The Phuoc Tan samples have lower Cs, Th, U, Zr, and LREE contents compared to rocks from other areas, which is probably due to the less evolved nature of this magma suite (lower SiO_2 content) and/or to the influence of alteration. One sample from the Phuoc Tan area (PT133) and one from the Vung Tau area (VT140), which have exceptionally high SiO_2

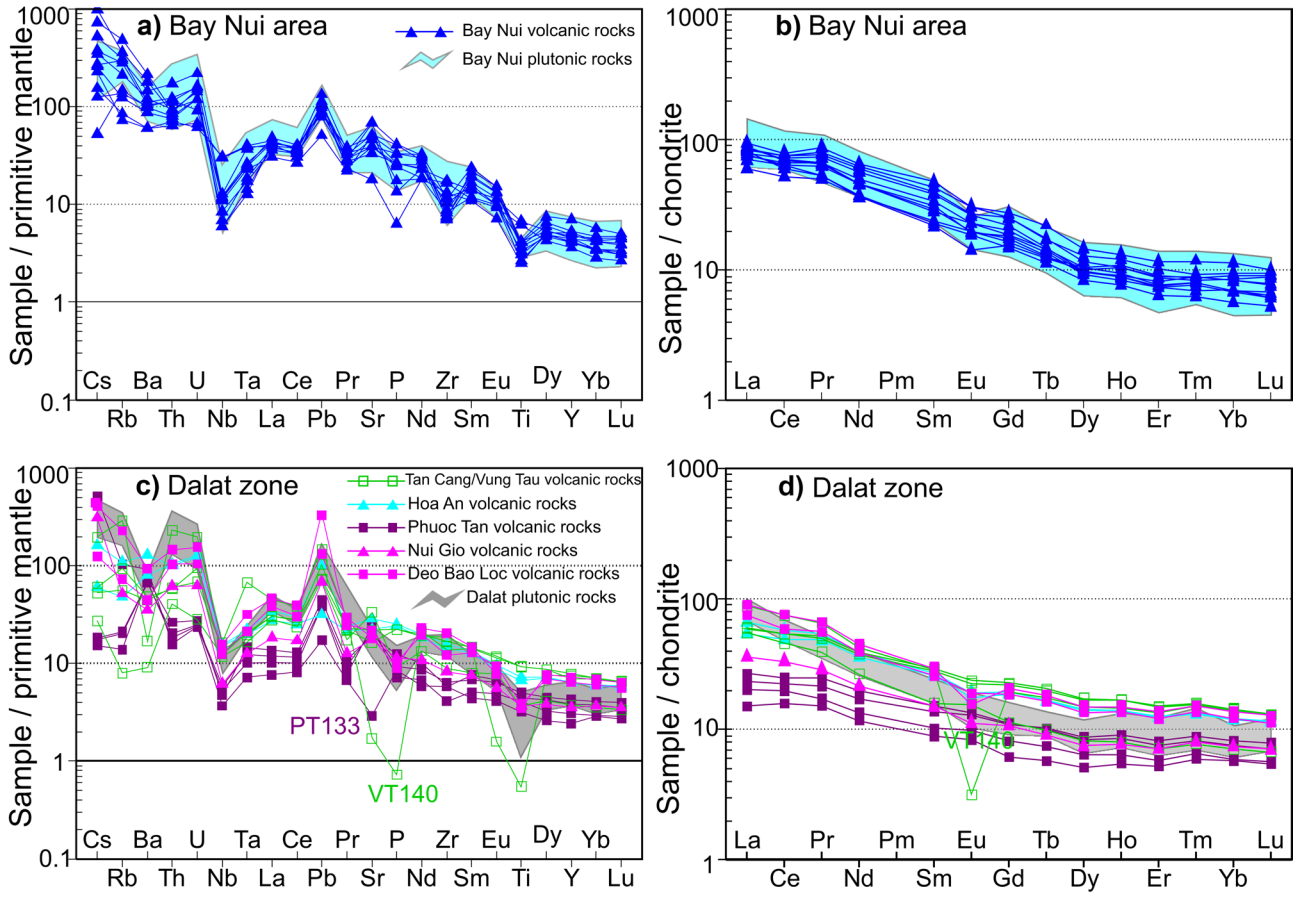

Fig. 7 Plots of primitive mantle-normalized trace elements (McDonough and Sun 1995) and chondrite-normalized REEs (Nakamura 1974): Samples from this study are plotted together with plutonic samples of equivalent silica content and the same age range (ca.100 Ma) occurring in the study area (i.e., Nguyen et al. 2004; Nong et al. 2021)

content clearly deviate from the common distribution trend of trace elements (Fig. 7c). In the tectonic classification diagrams (Fig. 8), most of the samples fall into the orogenic, volcanic arc basalt, calc-alkaline basalt, and typical arc rock fields (Pearce et al. 1977; Wood 1980; Defant and Drummond 1990; Pearce 2014).

Zircon U-Pb dating

Cathodoluminescence (CL) images of representative zircon grains from the volcanic rocks are presented in Fig. 9. Zircon U-Pb dates with discordance of less than 5% are presented on Wetherill concordia diagrams ($^{207}Pb/^{235}U$ versus $^{206}Pb/^{238}U$) for all age ranges and additional age-ranked weighted mean plots are shown for the young age group (ca. 100 Ma) (Fig. 10). The $^{206}Pb/^{238}U$ weighted mean ages were calculated from single zircon dates forming statistically robust plateaus. The uncertainty shown with the $^{206}Pb/^{238}U$ weighted mean age includes propagated systematic uncertainties. Raw data of zircon U-Pb dating is given in Supplementary Table S4 in the ESM.

Zircon grains of the different age groups display mildly distinct characteristics (morphology, internal structure, and zircon size). Three distinct age groups can be identified: ca. 100 Ma (group 1, 78 spots), ca. 250 Ma (group 2, 61 spots), and ca. 350 Ma (group 3, 24 spots). Zircon of group 1 is usually euhedral, small to medium in size (50–150 µm) and shows a distinct oscillatory growth zonation typical for magmatic zircon (Corfu et al. 2003). Zircon of group 2 is xenocrystic (sample BN97 and PT134) and is usually more variable in size (30–180 µm) compared to zircon of group 1. They display a multifaceted structure in the grain interiors and occasionally contain older xenocrystic cores (sample PT134). The zircon of group 3 is xenocrystic and has the smallest grain size of all zircon samples (30–100 µm) and partly destroyed crystal edges. Although zircon of the two latter groups is xenocrystic, they show oscillatory zonation and Th/U > 0.1, characteristic of a magmatic origin of their protoliths (Rubatto 2002). The majority of zircon grains in group 1 are pale pink or orange and transparent, whereas zircon in groups 2 and 3 are usually dark orange and less transparent. The $^{206}Pb/^{238}U$ weighted mean ages of the youngest age group (group 1) are interpreted as the eruption ages of

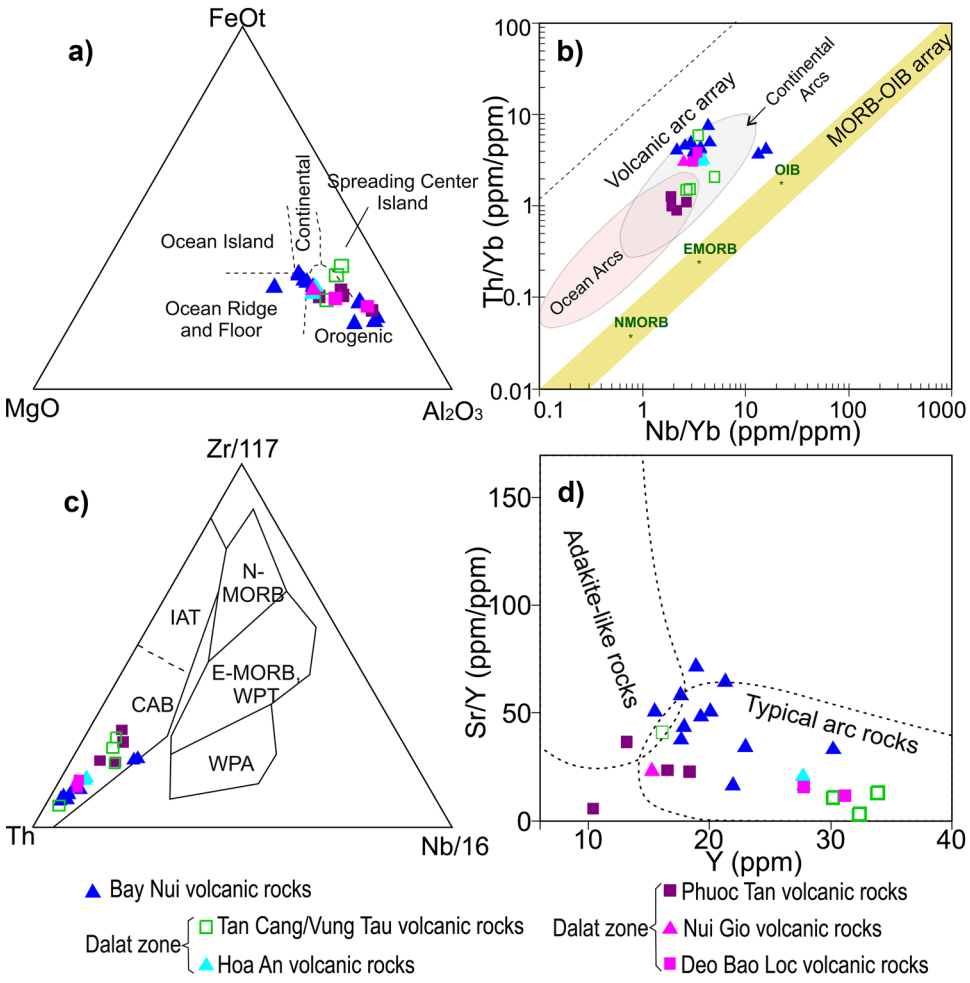

Fig. 8 Tectonic classification: **a** MgO-FeOt-Al_2O_3 diagram (Pearce et al. 1977); **b** Nb/Yb versus Th/Yb (Pearce 2014), **c** Triangular diagrams of Th, Zr/117, and Nb/16 (Wood 1980); and **d** Sr/Y versus Y diagram for distinguishing typical arc rocks from adakite-like rocks (Defant and Drummond 1990). Abbreviations: IAT–island-arc tholeiites, CAB–calc-alkaline basalts, N-MORB–N-type mid-ocean–ridge basalts, E-MORB–E-type mid-ocean–ridge basalts, WPA–alkaline within-plate basalts

the volcanic rocks while the old groups (group 2 and group 3) document earlier magmatic events.

Bay Nui basaltic andesite: Thirty-one zircon grains were analyzed for sample BN109. Twenty-seven spots are concordant and all belong to group 1 (Fig. 10a). The $^{206}Pb/^{238}U$ weighted mean age calculated from eighteen spots is 94.2 ± 1.3 Ma (n = 18, MSWD = 1.6). For sample BN97, forty-five zircon grains were dated and twenty-nine are concordant (Fig. 10b). Two main age groups are recorded: group 1 yielded $^{206}Pb/^{238}U$ dates from 101 to 127 Ma (Fig. 10b$_1$) and group 2 yielded a range between 216 and 263 Ma (Fig. 10b$_2$).

Fig. 10 U-Pb concordia diagrams of volcanic rocks for the old age groups (group 2 - ca. 250 Ma with yellow background and group 3 - ca. 350 Ma with light-blue background) in the Bay Nui area (BN109 and BN97) and Dalat zone (PT134, VT138, and DBL145) with weighted mean $^{206}Pb/^{238}U$ age diagrams for the young age group (group 1 - ca. 100 Ma). Uncertainties shown with the weighted mean age include systematic components (2 sigma level). Internal 2σ of the mean is shown for comparison

Phuoc Tan andesitic tuff: Fifty-two zircon grains of sample PT134 were analyzed and forty-seven are concordant (Fig. 10c). Two main age groups are recorded: group 1 yielded a $^{206}Pb/^{238}U$ weighted mean age of 101.8 ± 1.8 Ma

Fig. 9 Cathodoluminescence (CL) images of representative zircon from volcanic rocks in the Bay Nui area (BN109 and BN97) and Dalat zone (PT134, VT138, and DBL145)

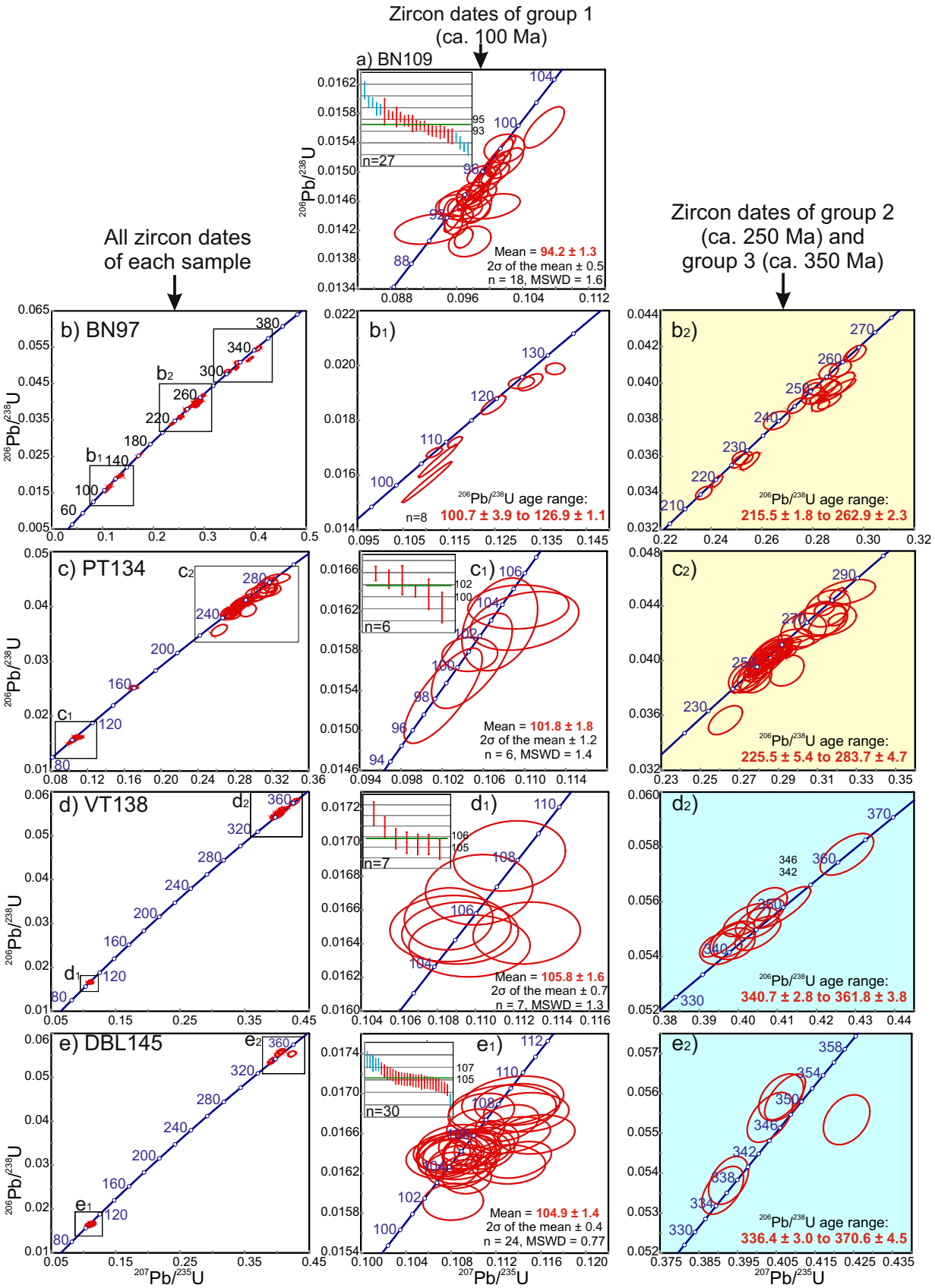
Zircon dates of group 1
(ca. 100 Ma)
a) BN109
Mean = 94.2 ± 1.3
2σ of the mean ± 0.5
n = 18, MSWD = 1.6
All zircon dates
of each sample
Zircon dates of group 2
(ca. 250 Ma) and
group 3 (ca. 350 Ma)
b) BN97
b1)
b2)
206Pb/238U age range:
100.7 ± 3.9 to 126.9 ± 1.1
215.5 ± 1.8 to 262.9 ± 2.3
c) PT134
c1)
c2)
Mean = 101.8 ± 1.8
2σ of the mean ± 1.2
n = 6, MSWD = 1.4
225.5 ± 5.4 to 283.7 ± 4.7
d) VT138
d1)
d2)
Mean = 105.8 ± 1.6
2σ of the mean ± 0.7
n = 7, MSWD = 1.3
340.7 ± 2.8 to 361.8 ± 3.8
e) DBL145
e1)
e2)
Mean = 104.9 ± 1.4
2σ of the mean ± 0.4
n = 24, MSWD = 0.77
336.4 ± 3.0 to 370.6 ± 4.5
206Pb/238U
207Pb/235U

(n = 6, MSWD = 1.4) (Fig. 10c$_1$) and group 2 yielded $^{206}Pb/^{238}U$ dates from 226 to 284 Ma (Fig. 10c$_2$).

Vung Tau andesite: Twenty-two zircon grains of the sample VT138 were analyzed and eighteen are concordant (Fig. 10d). Two main age groups are recorded: group 1 yielded a $^{206}Pb/^{238}U$ weighted mean age of 105.8 ± 1.6 Ma (n = 7, MSWD = 1.3) (Fig. 10d$_1$) and $^{206}Pb/^{238}U$ dates of another group (group 3) range from 341 to 361 Ma (Fig. 10d$_2$).

Deo Bao Loc andesite: Forty-two zircon grains of the sample DBL145 were analyzed and thirty-six are concordant (Fig. 10e). The majority of dated zircon grains belong to group 1 and yielded a $^{206}Pb/^{238}U$ weighted mean age of 104.9 ± 1.4 Ma (n = 24, MSWD = 0.77) (Fig. 10e$_1$). A few zircon grains of group 3 show $^{206}Pb/^{238}U$ dates ranging from 336 to 371 Ma (Fig. 10e$_2$).

Discussion

Magma differentiation

Several potential sources have been proposed for subduction-related magmas including the subducted slab, the overlying mantle wedge, and the deep continental and oceanic crust (Grove and Kinzler 1986; Schiano et al. 2010). Above subduction zones, calc-alkaline andesitic melts are generally supposed to be the product of fractional crystallization from basaltic magmas under hydrous conditions and their interaction with arc crust (Schiano et al. 2010) with crustal materials often contributing to some extent to the formation of andesitic lavas (DePaolo 1981; Bryant et al. 2006). Recently, Chen and Zhao (2017) suggested that source mixing (SARSH) is another possible mechanism for the generation of continental arc andesites explaining the incorporation of crustal-derived materials into the mantle source of andesitic magmas.

Volcanic rocks in the study area show a wide range of calc-alkaline magma compositions ranging from basaltic andesite to dacite (and rare rhyolite). Andesitic rocks in the Deo Bao Loc have been shown to be the product of fractionation of mantle-derived melts with a contribution of crustal components with initial $^{143}Nd/^{144}Nd$ ratios of 0.5123–0.5125, εNd = -3,07 to + 1.51, and initial $^{87}Sr/^{86}Sr$ ratios of 0.7041–0.7069 (Bao 2000; Tri and Khuc 2009).

Since isotopic compositions were not determined in this study, trace element contents were used to investigate the magmatic processes controlling the geochemical compositions of the studied volcanic rocks. Two highly incompatible elements (C^H) are plotted against each other (Th versus Rb) (Schiano et al. 2010) (Fig. 11a). In this plot, the majority of samples within a locality follow a fractional crystallization trend with exception of a few samples from the Dalat zone, which indicates that fractional crystallization played an important role during magma differentiation.

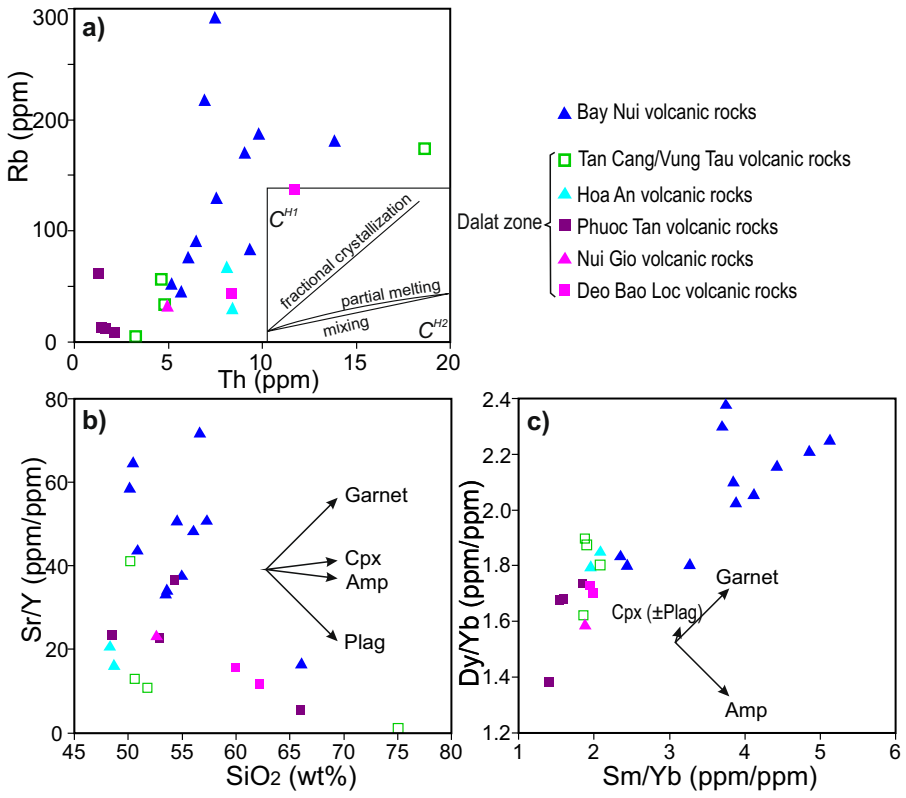

Fig. 11 Trace element variation diagrams to identify magmatic processes: **a** Two highly incompatible elements (C^H) are plotted against each other (Th versus Rb) (Schiano et al. 2010); **b** Sr/Y versus SiO_2 and **c** Sm/Yb versus Dy/Yb diagrams; **b** and **c** show fractionation of dominant phases during magma differentiation; abbreviations: Cpx – clinopyroxene, Plag – plagioclase, and Amp – amphibole

The Sr/Y versus SiO_2 and Dy/Yb versus Sm/Yb diagrams are used to investigate the phases determining the fractionation trends (Mamani et al. 2010; Wörner et al. 2018). The Sr/Y ratio is particularly sensitive to track the presence of plagioclase or garnet while the Dy/Yb and Sm/Yb ratios are sensitive to distinguish between amphibole and garnet, respectively, during high-pressure magma evolution with increasing crustal thickness through time (Mamani et al. 2010). At low pressures at shallow depth or within a thin arc crust, plagioclase and clinopyroxene tend to be the dominant fractionating phases, which causes the Sr/Y ratio to remain low. The Dalat rocks partly follow the amphibole fractionation trend (Fig. 11b) and subordinately the clinopyroxene (±plagioclase) trend (Fig. 11c), which indicates fractionation at a middle crustal level for some rocks and an upper crustal level or a thin-crust setting for other samples. In contrast, the Bay Nui rocks mainly follow a distinct garnet trend, which suggests that fractionation at greater depth is probably related to crustal thickening. Few samples of the Bay Nui area lie outside the field of typical arc rocks (Fig. 8d) due to elevated Sr (> 400 ppm) and lower Y contents (< 18 ppm) (Defant and Drummond 1990). The elevated Sr/Y ratio in these samples might be assigned to either differentiation of amphibole and/or garnet from wet basaltic magma at lower crustal levels or to fluid-related modifications seen also in elevated potassium contents (Macpherson et al. 2006; Rodríguez et al. 2007; Rooney et al. 2011).

Moreover, mineral chemistry is consistent with fractional crystallization. Oscillatory zonation of clinopyroxene might be explained by periodic changes in melt composition, pressure, or temperature (Shore and Fowler 1996; Schoneveld et al. 2020) (Fi. S1 in the ESM). Concentric zoning in plagioclase with decreasing X_{An} towards the rim reflects the development of more evolved magma over time, however, no rhythmic zoning - as observed in clinopyroxene - occurs.

Whole-rock chemical compositions with variable concentrations of highly incompatible trace elements (e.g., Rb, Cs, Ba, Pb, Th, and LREEs) might be explained by the assimilation of crustal material or addition of crust-derived melts to the andesitic melts. The stronger enrichment in LILE, particularly potassium, and LREE concentrations of rocks from the Bay Nui area compared to rocks from the Dalat zone is probably largely due to fractional crystallization. Therefore, besides fractional crystallization (Fig. 11), crustal contamination is regarded as an important process to explain the observed geochemical trends (Bryant et al. 2006). An alternative explanation for the abnormally high potassium content of samples from the Bay Nui area could be mantle-derived alkali-rich parental melts generated from partial melting of K-rich metasomatized lithospheric mantle containing amphibole and/or phlogopite (Conceiçao and Green 2004; Conticelli et al. 2009; Bucholz et al. 2014).

The general low Mg# (= 100*MgO/(MgO + FeO) = 19.9–41.4) and higher alkali contents of the studied samples compared to other andesites from continental arcs (Conway et al. 2020a, b) possibly result from either fractionation processes of the magma during ascent or, according to a recent interpretation, from source mixing and partial melting of metasomatic domains in the mantle wedge (Chen and Zhao 2017; Chen et al. 2021). Such metasomatic domains might result from the reaction of mantle wedge peridotite with hydrous felsic melts derived from the subducted slab.

From the magma differentiation trends and overall geochemical compositions of the studied rocks, two alternative schematic tectonic models can be proposed (Fig. S3 in the ESM): (1) "Basalt-input model" supporting the assumption that assimilation and fractional crystallization (AFC) processes account for the observed chemical compositions and (2) the SARSH model (Chen and Zhao 2017; Chen et al. 2021) interpreted as subduction, anatexis, reaction, storage and heating, which favors the hypothesis of source mixing and partial melting of metasomatic domains in the mantle wedge. The former is supported by bulk compositions ranging mainly from basaltic to andesitic and the evidence of fractional crystallization trends and assimilation that led to enrichment and variable concentrations of melt-mobile incompatible trace elements. The latter might better explain the enrichments of Rb, Cs, Ba, Pb, Th, and LREEs of the studied volcanic rocks and the addition of crustal components to primitive high-K arc melts.

Timing of eruption and significance of xenocrystic zircon

Kernel density estimate (KDE) plots of $^{206}Pb/^{238}U$ dates of single zircon grains from volcanic rocks clearly display three different populations at ca. 350 Ma, ca. 250 Ma, and ca. 100 Ma (Fig. 12a). These are observed both in the Bay Nui area and the Dalat zone (Phuoc Tan, Vung Tau, and Deo Bao Loc). The youngest age group (ca. 100 Ma) is considered to be the volcanic stage, which is consistent with the timing of Paleo-Pacific subduction-related magmatism, particularly with the so-called Late Yanshanian orogenic event reported along the eastern margin of China and Vietnam (Zhou and Li 2000; Nguyen et al. 2004; Thuy et al. 2004; Zhou et al. 2006; Shellnutt et al. 2013; Nong et al. 2021). Field relationships also support the magmatic ages obtained in this study (Tong et al. 2011) as volcanic rocks unconformably overlie formations of the Devonian and Jurassic ages. They contain xenoliths of Late Mesozoic granitoids (ca.106 Ma) at the Bay Nui area (Nong et al. 2021) and agree with the age range of 100–128 Ma derived from K-Ar and Ar-Ar whole-rock dating results (Bao 2000). Volcanism in southern Vietnam is spatially distributed within and

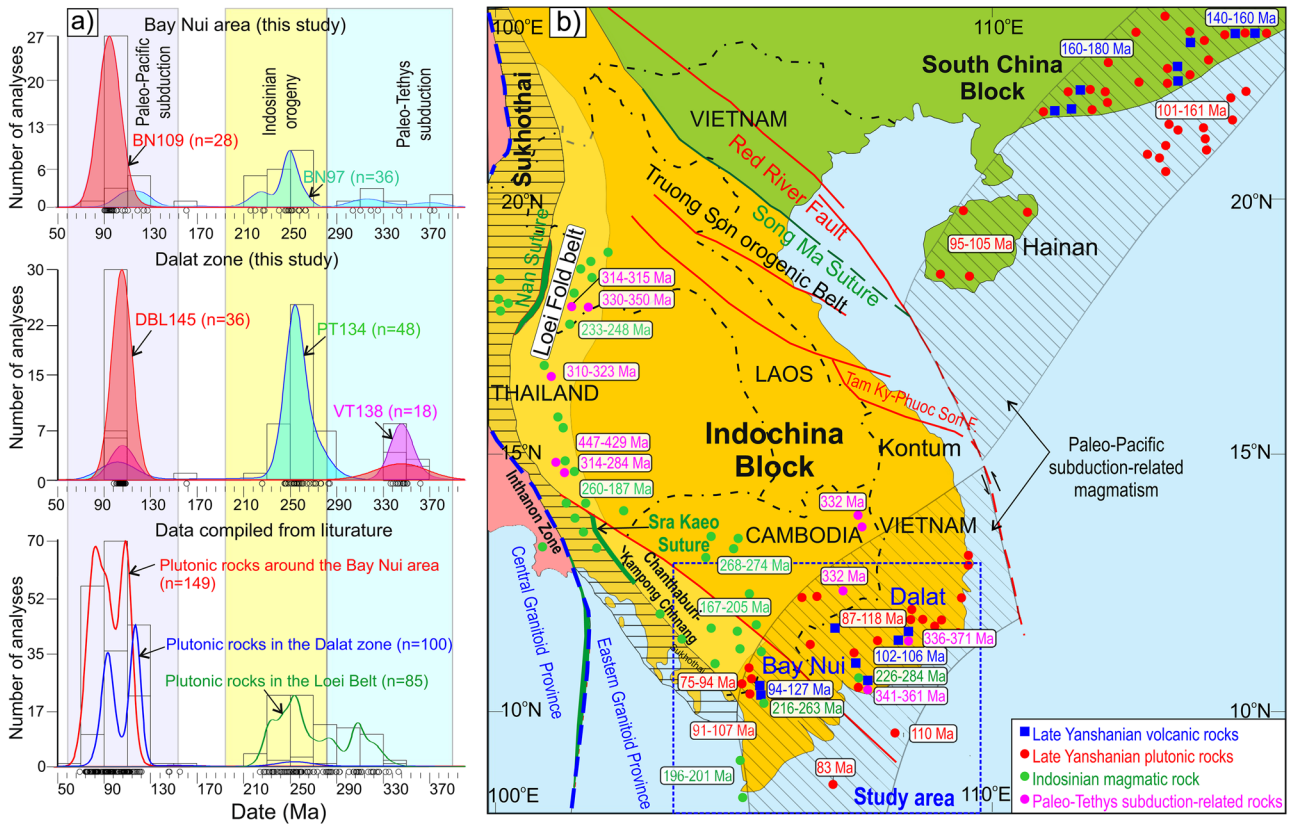

Fig. 12 **a** Kernel density estimate (KDE) plots of zircon $^{206}Pb/^{238}U$ dates from this study and compiled dates of representative plutonic rocks in the study area and vicinity (Nguyen et al. 2004; Shellnutt et al. 2013; Fanka et al. 2018; Nong et al. 2021); **b** Schematic map summarizing the distribution of representative Late Paleozoic and Mesozoic volcanic-plutonic assemblages in southern Vietnam and adjacent areas

temporally coeval with the Late Mesozoic Paleo-Pacific subduction-related granitoid belt and coincides with Late Mesozoic volcanism in southeastern China.

Figure 12b summarizes the emplacement ages of Mesozoic volcanic rocks obtained in this study, Late Paleozoic-Early Mesozoic rocks (Fanka et al. 2018; Nualkhao et al. 2018; Cheng et al. 2019; Hunyek et al. 2020; Nong et al. 2022) and Late Mesozoic rocks are compiled from the literature (Nguyen et al. 2004; Zhou et al. 2006; Shellnutt et al. 2013; Xu et al. 2016; Yan et al. 2017; Cheng et al. 2019; Nong et al. 2021). Volcanism and plutonism along western Indochina occurred episodically from the Carboniferous to the Triassic in the Loei Fold Belt and Sukhothai arc (Zaw and Meffre 2007, Zaw et al. 2014; Fanka et al. 2018; Hunyek et al. 2020). These magmatic episodes correlate with (1) the subduction of Paleo-Tethys beneath the western margin of Indochina and (2) the plate amalgamation of Sibumasu and Indochina during the Indosinian orogeny (Fig. 12a). Thus, U-Pb age data obtained from zircon xenocrysts in this study (336–371 Ma and 216–284 Ma) indicate that these magmatic events had some influence on the eastern edge of Indochina.

Further to the north of the study area, within the Kontum massive and the Song Ma Suture Zone, the ~250 Ma magmatic rocks are widespread and have been linked to the amalgamation of South China and Indochina referred to as Indosinian orogeny (Hieu et al. 2015). This magmatism is supposed to have taken place at approximately the same time as the Simumasu-Indochina amalgamation. We cannot firmly ascribe xenocrystic zircon to whether Sibumasu-Indochina or Indochina-South China amalgamation. Nevertheless, from compiled age data throughout eastern Thailand and southern Cambodia (Fig. 12b), an explicit continuity of Early Mezozoic magmatic belts, as well as another episode of Late Paleozoic (i.e., Carboniferous) volcanism can be observed within the Loei Fold Belt which extends southward into southeastern Cambodia and southernmost Vietnam. The spatial distribution of this magmatism further supports the correlations between xenocrystic zircon dates of the studied volcanic rocks and magmatism associated with the convergent tectonics and later Indosinian orogeny along the western margin of Indochina.

Volcanic-plutonic connection and correlation of Late Mesozoic volcanism with the regional framework of the Paleo-Pacific subduction

Pyroxene, amphibole, and whole-rock compositions (trace and rare earth elements) of volcanic rocks in southern Vietnam are similar to those of the plutonic rocks of equivalent silica concentration in the study area (Figs. 6a and c and 7). Similar trace element patterns of volcanic and plutonic rocks have been found in a previous study of global arc magmas and might indicate that both rock groups derive from the same magma (Glazner et al. 2015). Additionally, the elevated potassium content of both plutonic and related volcanic rocks from the Bay Nui area may indicate that they were both derived from an alkali-rich primitive arc melt that experienced similar differentiation paths before emplacement/eruption. Compared with igneous rocks from the Bay Nui area, the Dalat plutonic and volcanic rocks are only moderately alkaline, which may indicate a common parental calc-alkaline melt. The connection between volcanics and plutonics in the Dalat zone is further supported by isotopic ratios of plutonics (initial $^{143}Nd/^{144}Nd = 0.5124–0.5126$, $\varepsilon Nd = -3.3 - +0.9$, initial $^{87}Sr/^{86}Sr = 0.7049–0.7069$, Nguyen 2003) that well overlap with those of volcanic rocks (Bao 2000; Tri and Khuc 2009). The similarities in chemical composition and crystallization ages (ca. 100 Ma) between volcanic and plutonic rocks in southern Vietnam suggest that they both formed during the Late Mesozoic Paleo-Pacific subduction.

To the north of Indochina, Late Mesozoic magmatism related to the Paleo-Pacific subduction has been studied in southeastern South China. Magmatic rocks characterized by calc-alkaline arc-like affinity are found to spatially coexist with A-type granites, shoshonite zones and minor Late Cretaceous basalts of a back-arc basin environment (Zhou et al. 2006). Together, they constitute an assemblage characteristic for an active continental arc system and a transitional phase to an extensional setting during the Jurassic-Cretaceous time. In terms of geochemical and geochronological characteristics, the studied volcanic rocks in southern Vietnam with arc-like affinity can be well correlated with widespread typical Late Mesozoic magmatism in southeastern South China that took place during the late stage of the Paleo-Pacific subduction (Late Yashanian Orogeny).

To the south of Indochina, Paleo-Pacific subduction-related magmatism has also been reported in Borneo Island (not shown on the map) and formed a large igneous province (Breitfeld et al. 2020). In that area, episodic Triassic-Late Cretaceous plutonics formed in alternate arc-like and extensional environments. During the Cretaceous, magmatism in Borneo Island has also been found to be multi-phased with four clusters of zircon dates: ca. 130 Ma, 115 Ma, 100 Ma, and 90 Ma interpreted as subduction-related magmatism and ca. 80 Ma and 70 Ma representative of extension-related magmatism.

Within the tectonic framework of the eastern margin of Asia (from southeast China to Borneo), volcanics in Vietnam are presumably temporally correlated with the transition from a late stage of Paleo-Pacific subduction to an extensional environment (Shellnutt et al. 2013; Nong et al. 2021). Primitive arc-related melts formed in this subduction setting underwent fractional crystallization and crustal contamination during crustal ascent and either erupted at the surface as volcanics or, more commonly, were emplaced as plutonic rocks in the upper crust as the Dinhquan or Bay Nui-Ba Den suites (Nguyen et al. 2004; Shellnutt et al. 2013; Nong et al. 2021).

Conclusions

Late Mesozoic volcanic rocks in southern Vietnam display a wide range in chemical compositions and lithological appearances. Major elements of mineral and whole-rock compositions clearly indicate a calc-alkaline affinity, and enrichment in LILEs and depletion in HFSEs resemble signatures of arc magmas.

The dominant fractional crystallization and an additional contribution of crustal material to the andesitic melts controlled the chemical composition of the studied volcanic rocks. Volcanic rocks in the Bay Nui area are likely more evolved or assimilated more crustal material compared to similar rocks in the Dalat zone. Volcanic rocks and plutonic rocks in southern Vietnam might derive from the same source based on the observed similarities in chemical compositions and the coincidence of ages.

The eruption ages of volcanic rocks obtained from the youngest zircon population are consistent with Paleo-Pacific subduction at ~ 100 Ma (Late Yanshanian orogenic event). Earlier magmatic events in this region (~ 350 Ma and ~ 250 Ma) are revealed by zircon xenocrysts and are probably linked to Paleo-Tethys subduction along the western margin of Indochina and to the Indosinian orogeny.

Supplementary information The online version contains supplementary material available at https://doi.org/10.1007/s00710-022-00785-z.

Acknowledgements We would like to thank Dominik Sorger for supporting us with the analytical process and for assisting with field work and Hoang Nguyen and Hieu Pham for precious recommendations and constructive discussions. We kindly acknowledge the technical support of the Graz University of Technology for laser ablation (MC) ICP-MS analyses. Constructive reviews by Xiaolei Wang and an anonymous expert, and insightful suggestions by editors Qiang Wang and Lutz Nasdala, are gratefully acknowledged. The study is part of the PhD research financed by the Ernst Mach-Grants (EMG) – ASEA-UNINET, the Austrian Agency for International Cooperation in Education & Research (OeAD GmbH) and research funds by C.A.H.

Funding Open access funding provided by University of Graz.

References

Abdel-rahman AFM (1994) Nature of biotites from alkaline, calc-alkaline, and peraluminous magmas. J Petrol 35:525–541

Anderson AT (1976) Magma mixing: petrological process and volcanological tool. J Volcanol Geotherm Res 1:3–33

Bao NX (2000) Tectonics and metallogeny of southern Vietnam. South Vietnam Geological Mapping Division (in Vietnamese), Hochiminh

Breitfeld HT, Davies L, Hall R et al (2020) Mesozoic Paleo-Pacific Subduction Beneath SW Borneo: U-Pb Geochronology of the Schwaner Granitoids and the Pinoh Metamorphic Group. Front Earth Sci 8:536

Bryant JA, Yogodzinski GM, Hall ML et al (2006) Geochemical constraints on the origin of volcanic rocks from the Andean Northern volcanic zone, Ecuador. J Petrol 47:1147–1175

Bucholz CE, Jagoutz O, Schmidt MW, Sambuu O (2014) Phlogopite- and clinopyroxene-dominated fractional crystallization of an alkaline primitive melt: petrology and mineral chemistry of the Dariv Igneous Complex, Western Mongolia. Contrib to Mineral Petrol 167:1–28

Chen L, Zhao ZF (2017) Origin of continental arc andesites: The composition of source rocks is the key. J Asian Earth Sci 145:217–232

Chen L, Zheng YF, Xu Z, Zhao ZF (2021) Generation of andesite through partial melting of basaltic metasomatites in the mantle wedge: Insight from quantitative study of Andean andesites. Geosci Front 12:101124

Cheng, R, Uchida, E, Katayose, M, Yarimizu, K, Shin, KC, Kong, S, & Nakano, T (2019) Petrogenesis and tectonic setting of Late Paleozoic to Late Mesozoic igneous rocks in Cambodia. J Asian Earth Sci 185:104046

Clements B, Burgess PM, Hall R, Cottam MA (2011) Subsidence and uplift by slab-related mantle dynamics: A driving mechanism for the Late Cretaceous and Cenozoic evolution of continental SE Asia? Geol Soc Spec Publ 355:37–51

Conceiçao RV, Green DH (2004) Derivation of potassic (shoshonitic) magmas by decompression melting of phlogopite + pargasite lherzolite. Lithos 72:209–229

Conticelli S, Guarnieri L, Farinelli A et al (2009) Trace elements and Sr–Nd–Pb isotopes of K-rich, shoshonitic, and calc-alkaline magmatism of the Western Mediterranean Region: Genesis of ultrapotassic to calc-alkaline magmatic associations in a post-collisional geodynamic setting. Lithos 107:68–92

Conway CE, Chamberlain KJ, Harigane Y et al (2020a) Rapid assembly of high-Mg andesites and dacites by magma mixing at a continental arc stratovolcano. Geology 48:1033–1037

Conway CE, Chamberlain KJ, Harigane Y et al (2020b) High-magnesian andesite from Mount Shasta: A product of magma mixing and contamination, not a primitive mantle melt. Geology 48:1033–1037

Corfu F, Hanchar JM, Hoskin PWO, Kinny P (2003) Atlas of zircon textures. Rev Mineral Geochemistry 53:469–500

Defant MJ, Drummond MS (1990) Derivation of some modern arc magmas by melting of young subducted lithosphere. Nature 347:662–665

DePaolo DJ (1981) Trace element and isotopic effects of combined wallrock assimilation and fractional crystallization. Earth Planet Sci Lett 53:189–202

Eichelberger JC (1978) Andesites in island arcs and continental margins: Relationship to crustal evolution. Bull Volcanol 41:480–500

Fanka A, Tsunogae T, Daorerk V et al (2018) Petrochemistry and zircon U-Pb geochronology of granitic rocks in the Wang Nam Khiao area, Nakhon Ratchasima, Thailand: Implications for petrogenesis and tectonic setting. J Asian Earth Sci 157:92–118

Fyhn MBW, Green PF, Bergman SC et al (2016) Cenozoic deformation and exhumation of the Kampot Fold Belt and implications for south Indochina tectonics. J Geophys Res Solid Earth 121:5278–5307

Glazner AF, Coleman DS, Mills RD (2015) The Volcanic-Plutonic Connection. Advances in Volcanology. Springer, Cham, pp 61–82

Grove TL, Kinzler RJ (1986) Petrogenesis of andesites. Annu Rev Earth Planet Sci 14:417–454

Hall R (2012) Late Jurassic–Cenozoic reconstructions of the Indonesian region and the Indian Ocean. Tectonophysics 570:1–41

Hawthorne FC, Oberti R, Harlow GE et al (2012) Ima report: Nomenclature of the amphibole supergroup. Am Mineral 97:2031–2048

Hieu PT, Yang YZ, Binh DQ et al (2015) Late Permian to Early Triassic crustal evolution of the Kontum massif, central Vietnam: Zircon U-Pb ages and geochemical and Nd-Hf isotopic composition of the Hai Van granitoid complex. Int Geol Rev 57:1877–1888

Hoa NN, Cau DV, Phan DN et al (1996) Geology and mineral resources map of Vietnam, scale 1:200,000. Department of geology and minerals of Vietnam, Hanoi. (in Vietnamese)

Horstwood MSA, Košler J, Gehrels G et al (2016) Community-Derived Standards for LA-ICP-MS U-(Th-)Pb Geochronology – Uncertainty Propagation, Age Interpretation and Data Reporting. Geostand Geoanalytical Res 40:311–332

Hunyek V, Sutthirat C, Fanka A (2020) Magma genesis and arc evolution at the Indochina Terrane subduction: petrological and geochemical constraints from the volcanic rocks in Wang Nam Khiao Area, Nakhon Ratchasima, Thailand. Front Earth Sci 8:271

Irvine TN, Baragar WRA (1971) A guide to the chemical classification of the common volcanic rocks. Can J Earth Sci 8:523–548

Jackson SE, Pearson NJ, Griffin WL, Belousova EA (2004) The application of laser ablation-inductively coupled plasma-mass spectrometry to in situ U-Pb zircon geochronology. Chem Geol 211:47–69

Janoušek V, Farrow CM, Erban V (2006) Interpretation of whole-rock geochemical data in igneous geochemistry: Introducing Geochemical Data Toolkit (GCDkit). J Petrol 47:1255–1259

Kamvong T, Zaw K, Meffre S et al (2014) Adakites in the Truong Son and Loei fold belts, Thailand and Laos: Genesis and implications for geodynamics and metallogeny. Gondwana Res 26:165–184

Le Bas MJ, Le Maitre RW, Streckeisen A, Zanettin B (1986) A chemical classification of volcanic rocks based on the total alkali-silica diagram. J Petrol 27:745–750

Leake BE, Woolley AR, Arps CES et al (1997) Nomenclature of amphiboles: Report of the subcommittee on amphiboles of the international mineralogical association, commission on new minerals and mineral names. Can Mineral 35:219–246

Leterrier J, Maury RC, Thonon P et al (1982) Clinopyroxene composition as a method of identification of the magmatic affinities of paleo-volcanic series. Earth Planet Sci Lett 59:139–154
Liu JX, Wang S, Wang XL et al (2020) Refining the spatio-temporal distributions of Mesozoic granitoids and volcanic rocks in SE China. J Asian Earth Sci 201:104503
Ludwig KR (2008) User's Manual for Isoplot 3.6: Geochronological Toolkit for Microsoft. Berkeley Geochronology Center Special Publication 4:78
Macpherson CG, Dreher ST, Thirlwall MF (2006) Adakites without slab melting: High pressure differentiation of island arc magma, Mindanao, the Philippines. Earth Planet Sci Lett 243:581–593
Mamani M, Wörner G, Sempere T (2010) Geochemical variations in igneous rocks of the Central Andean orocline (13°S to 18°S): Tracing crustal thickening and magma generation through time and space. Bull Geol Soc Am 122:162–182
McDonough WF (1991) Partial melting of subducted oceanic crust and isolation of its residual eclogitic lithology. Philos Trans - R Soc London A 335:407–418
McDonough WF, Sun S-S (1995) The composition of the Earth. Chem Geol 120:223–253
Metcalfe I (2017) Tectonic evolution of Sundaland. Bull Geol Soc Malaysia 63:27–60
Morimoto N (1988) Nomenclature of Pyroxenes. Mineral Petrol 39:55–76
Morley CK (2012) Late Cretaceous-Early Palaeogene tectonic development of SE Asia. Earth Sci Rev 115:37–75
Nakamura N (1974) Determination of REE, Ba, Fe, Mg, Na and K in carbonaceous and ordinary chondrites. Geochim Cosmochim Acta 38:757–775
Nasdala L, Hofmeister W, Norberg N et al (2008) Zircon M257 - A homogeneous natural reference material for the ion microprobe U-Pb analysis of zircon. Geostand Geoanalytical Res 32:247–265
Nguyen TTB (2003) Geochemistry and Geochronology of Granitoids in the Dalat Zone, South Vietnam: Implications for the Mesozoic Circum-Pacific Magnetism and Conclusions on the Genesis of Tin Deposits. PhD Dissertation, Eberhard Karls University of Tübingen
Nguyen TTB, Satir M, Siebel W, Chen F (2004) Granitoids in the Dalat zone, southern Vietnam: age constraints on magmatism and regional geological implications. Int J Earth Sci 93:329–340
Nong ATQ, Hauzenberger CA, Gallhofer D, Dinh SQ (2021) Geochemistry and zircon U Pb geochronology of Late Mesozoic igneous rocks from SW Vietnam – SE Cambodia: Implications for episodic magmatism in the context of the Paleo-Pacific subduction. Lithos 390–391:106101
Nong ATQ, Hauzenberger CA, Gallhofer D et al (2022) Early Mesozoic granitoids in southern Vietnam and Cambodia: A continuation of the Eastern Province granitoid belt of Thailand. J Asian Earth Sci 224:105025
Nualkhao P, Takahashi R, Imai A, Charusiri P (2018) Petrochemistry of Granitoids Along the Loei Fold Belt, Northeastern Thailand. Resour Geol 68:395–424
Paton C, Woodhead JD, Hellstrom JC et al (2010) Improved laser ablation U-Pb zircon geochronology through robust downhole fractionation correction. Geochem Geophys Geosyst. https://doi.org/10.1029/2009GC002618
Paton C, Hellstrom J, Paul B et al (2011) Iolite: Freeware for the visualisation and processing of mass spectrometric data. J Anal At Spectrom 26:2508–2518
Pearce TH, Gorman BE, Birkett TC (1977) The relationship between major element chemistry and tectonic environment of basic and intermediate volcanic rocks. Earth Planet Sci Lett 36:121–132
Pearce JA (2014) Immobile element fingerprinting of ophiolites. Elements 10:101–108
Peccerillo A, Taylor SR (1976) Geochemistry of Eocene calc-alkaline volcanic rocks from the Kastamonu area, northern Turkey. Contrib to Mineral Petrol 58:63–81
Rodríguez C, Sellés D, Dungan M et al (2007) Adakitic dacites formed by intracrustal crystal fractionation of water-rich parent magmas at Nevado de Longaví volcano (36.2°S; Andean Southern Volcanic Zone, Central Chile). J Petrol 48:2033–2061
Rooney TO, Franceschi P, Hall CM (2011) Water-saturated magmas in the Panama Canal region: A precursor to adakite-like magma generation? Contrib to Mineral Petrol 161:373–388
Rubatto D (2002) Zircon trace element geochemistry: Partitioning with garnet and the link between U-Pb ages and metamorphism. Chem Geol 184:123–138
Schiano P, Monzier M, Eissen JP et al (2010) Simple mixing as the major control of the evolution of volcanic suites in the Ecuadorian Andes. Contrib to Mineral Petrol 160:297–312
Schoneveld L, Barnes SJ, Makkonen HV et al (2020) Zoned Pyroxenes as Prospectivity Indicators for Magmatic Ni-Cu Sulfide Mineralization. Front Earth Sci 8:256
Shellnutt JG, Lan CY, Van Long T et al (2013) Formation of Cretaceous Cordilleran and post-orogenic granites and their microgranular enclaves from the Dalat zone, southern Vietnam: Tectonic implications for the evolution of Southeast Asia. Lithos 182–183:229–241
Shore M, Fowler AD (1996) Oscillatory zoning in minerals: A common phenomenon. Can Mineral 34:1111–1126
Sláma J, Košler J, Condon DJ et al (2008) Plešovice zircon - A new natural reference material for U-Pb and Hf isotopic microanalysis. Chem Geol 249:1–35
Sone M, Metcalfe I (2008) Parallel Tethyan sutures in mainland Southeast Asia: New insights for Palaeo-Tethys closure and implications for the Indosinian orogeny. Comptes Rendus - Geosci 340:166–179
Tatsumi Y, Sato T, Kodaira S (2015) Evolution of the Earth as an andesite planet: Water, plate tectonics, and delamination of anticontinent Planetary science. Earth Planet Sp 67:1–10
Thuy NTB, Satir M, Siebel W et al (2004) Geochemical and isotopic constraints on the petrogenesis of granitoids from the Dalat zone, southern Vietnam. J Asian Earth Sci 23:467–482
Tien PC (1991) Geological Map of Cambodia, Laos and Vietnam, Central Vietnam, Map sheet 1: 1 000 000, with explanatory note (in Vietnamese and English). Geological Survey of Vietnam, Hanoi, Vietnam
Tong DT, Vũ K, Boucot AJ (2011) Stratigraphic Units of Vietnam. Vietnam National University Publishing House, Hanoi, pp 1–566
Tri TV, Khuc V (2009) Geology and natural resources of Vietnam. Natural Science and Technology Publishing House, Hanoi
Whitney DL, Evans BW (2010) Abbreviations for names of rock-forming minerals. Am Mineral 95:185–187
Wiedenbeck M, Allé P, Corfu F et al (1995) Three Natural Zircon Standards for U-Th-Pb, Lu-Hf, Trace Element and Ree Analyses. Geostand Newsl 19:1–23
Winchester JAA, Floyd PAA (1977) Geochemical discrimination of different magma series and their differentiation products using immobile elements. Chem Geol 20:325–343
Wood DA (1980) The application of a Th–Hf–Ta diagram to problems of tectonomagmatic classification and to establishing the nature of crustal contamination of basaltic lavas of the British Tertiary Volcanic Province. Earth Planet Sci Lett 50:11–30
Wörner G, Mamani M, Blum-Oeste M (2018) Magmatism in the central andes. Elements 14:237–244
Xu C, Shi H, Barnes CG, Zhou Z (2016) Tracing a late Mesozoic magmatic arc along the Southeast Asian margin from the granitoids drilled from the northern South China Sea. Int Geol Rev 58:71–94
Yan Q, Metcalfe I, Shi X (2017) U-Pb isotope geochronology and geochemistry of granites from Hainan Island (northern South China

Sea margin): Constraints on late Paleozoic-Mesozoic tectonic evolution. Gondwana Res 49:333–349
Zaw K, Meffre S (2007) Metallogenic Relations and Deposit Scale Studies, Final Report: Geochronology, Metallogenesis and Deposit Styles of Loei Fold Belt in Thailand and Laos PDR. University of Tasmania, Hobart
Zaw K, Meffre S, Lai CK et al (2014) Tectonics and metallogeny of mainland Southeast Asia - A review and contribution. Gondwana Res 26:5–30
Zheng YF (2019) Subduction zone geochemistry. Geosci Front 10:1223–1254
Zhou XM, Li WX (2000) Origin of late Mesozoic igneous rocks in Southeastern China: Implications for lithosphere subduction and underplating of mafic magmas. Tectonophysics 326:269–287
Zhou X, Sun T, Shen W et al (2006) Petrogenesis of Mesozoic granitoids and volcanic rocks in South China: A response to tectonic evolution. Episodes 29:26–33